Exp Brain Res (2015) 233:735–749
DOI 10.1007/s00221-014-4151-2

RESEARCH ARTICLE

Modulation of intrinsic and reflexive contributions to low-back stabilization due to vision, task instruction, and perturbation bandwidth

P. van Drunen · Y. Koumans · F. C. T. van der Helm · J. H. van Dieën · R. Happee

Received: 27 July 2014 / Accepted: 15 November 2014 / Published online: 8 January 2015

Abstract The goal of this study is to assess how reflexes and intrinsic properties contribute to low-back stabilization and modulate with conditions. Upper body sway was evoked by anterior–posterior platform translations, while subjects were seated with a restrained pelvis and free upper body. Kinematic analysis of trunk translations and rotations illustrated that a fixed rotation point between the vertebrae L4 and L5 adequately captures lumbar bending up to 5 Hz. To investigate the motor control modulation, the conditions varied in vision (eyes open or closed), task instruction (*Balance* naturally or *Resist* perturbations by minimizing low-back motions), and perturbation bandwidth (from 0.2 up to 1, 3 or 10 Hz). Frequency response functions and physiological modeling parameters showed substantial modulation between all conditions. The eyes-open condition led to trunk-in-space behavior with additional long-latency visual feedback and decreased proprioceptive feedback. The task instruction to resist led to trunk-on-pelvis stabilization behavior, which was achieved by higher co-contraction levels and increased reflexive velocity feedback. Perturbations below the low-back natural frequency (~1 Hz) led to trunk-on-pelvis stabilization behavior, mainly attributed to increased intrinsic damping. This indicates that bandwidth effects should not be ignored and that experiments with high-bandwidth perturbations do not fully represent the intrinsic and reflexive behavior during most (low-bandwidth) daily life activities. The neck stabilized the head orientation effectively (head rotation amplitudes 2 % of trunk), but did not effectively stabilize the head in space (global head translations exceeded trunk translations by 20 %). This indicates that low-back motor control is involved in head-in-space stabilization and could explain the low-back motor control modulations due to vision.

Keywords Lumbar spine · Postural control · System identification · Muscle spindles · Head stabilization

Abbreviations

LBP	Low-back pain
FRF	Frequency response functions
RMS	Root mean square
$\gamma^2(f)$	Coherence
VAF	Variance accounted for
SEM	Standard error of the mean

Conditions

BT	Task instruction to balance naturally
B1	Perturbation signal with bandwidth of 0.2–1 Hz
B3	Perturbation signal with bandwidth of 0.2–3 Hz
B10	Perturbation signal with bandwidth of 0.2–10 Hz
EC	Eyes-closed conditions
EO	Eyes-open conditions
RT	Task instruction to resist the perturbation by minimizing flexion/extension excursions

Signals

$P(t)$	Perturbation signal
$X_{GT}(t)$	Global torso translations

P. van Drunen (✉) · Y. Koumans · F. C. T. van der Helm · R. Happee
BioMechanical Engineering Department, Faculty of Mechanical Engineering, Delft University of Technology, Mekelweg 4, 2628 CD Delft, The Netherlands
e-mail: P.vanDrunen@TUDelft.nl

J. H. van Dieën
Faculty of Human Movement Sciences, MOVE Research Institute Amsterdam, VU University Amsterdam, van der Boechorststraat 9, 1081 BT Amsterdam, The Netherlands

$X_{RT}(t)$	Relative torso translations
$\theta_T(t)$	Torso rotations
$X_{GH}(t)$	Global head translations
$X_{RH}(t)$	Relative head translations
$\theta_H(t)$	Head rotations
$E(t)$	EMG signal
$X(f)$	FRF of translations
$\theta(f)$	FRF of rotations
$E(f)$	FRF of EMG
$\theta_{mdl}(t)$	Estimated model rotations
$E_{mdl}(t)$	Estimated model EMG

Model parameters

m	Mass (model)
h	Pendulum height (model)
b	Intrinsic damping (model)
k	Intrinsic stiffness (model)
k_v	Reflexive velocity feedback gain (model)
k_p	Reflexive position feedback gain (model)
τ_{ref}	Reflexive time delay (model)
f_{act}	Muscle activation cutoff frequency (model)
d_{act}	Muscle activation damping factor (model)
e_{scale}	EMG scaling parameter (model)
k_{vis}	Visual position feedback gain (model)
τ_{vis}	Visual time delay (model)

Introduction

Low-back pain (LBP) is a common disorder affecting 40–60 % of the adult population in Western society annually (Loney and Stratford 1999; Picavet and Schouten 2003). Motor control deficits (e.g., increased co-contraction, delayed reflexes) have been suggested as potential cause or effect of LBP and its recurrent behavior (Cholewicki et al. 2000; Radebold et al. 2001; van Dieën et al. 2003). However, much is still unknown about the lumbar motor control in healthy subjects.

Humans maintain an upright posture and stabilize the trunk with proprioceptive, visual and vestibular feedback, and intrinsic muscle properties including co-contraction (Brown and McGill 2008; Moorhouse and Granata 2007). Most studies on low-back stabilization have focused either on the intrinsic muscle properties (Brown and McGill 2009; Gardner-Morse and Stokes 2001) or on reflexes [e.g., Radebold et al. (2001)], leading to potentially incorrect estimates, because changes in co-contraction could result in changes in estimated reflex properties and vice versa. Only a few studies quantified both the reflexive and the intrinsic contributions to low-back stabilization, by mechanical force perturbations to the trunk in anterior–posterior direction (Granata and Rogers 2007; van Drunen et al. 2013) or by rotational platform perturbation in lateral direction (Goodworth and Peterka 2009, 2010).

Low-back stabilization can generally be described as trunk-in-space or trunk-on-pelvis stabilization strategies. Trunk-in-space stabilization minimizes translations of the trunk in space (which is essential for daily upper extremity tasks) and minimizes head motion in space (beneficial for visual perception and motion-related comfort). Trunk-on-pelvis stabilization minimizes lumbar bending which is related to slow and/or large pelvis motions such as in walking. Proprioception and intrinsic properties effectively minimize lumbar bending and thus support trunk-on-pelvis stabilization. On the other hand, visual and vestibular feedback is more suitable for head-in-space and/or trunk-in-space stabilization. Stabilization strategy adaptation and thus low-back motor control modulation is essential to be able to operate with altering conditions or tasks. Compare, for example, stabilizing the trunk while lifting a heavy load as in power lifting with that when moving rapidly over uneven terrain as in mogul skiing. This study focusses on changes due to vision, task instructions, and perturbation bandwidth.

Vision has been related to a strategy decreasing overall musculoskeletal stiffness by a decrease in intrinsic stiffness and/or proprioceptive and/or vestibular feedback during standing balance control (Collins and De Luca 1995). Small vision effects were found for low-back stabilization in the frontal plane (Goodworth and Peterka 2009), while vision during high-bandwidth perturbations resulted in a consistent change to a head and trunk-in-space strategy in anterior–posterior stabilization studies on the neck (Forbes et al. 2013) and in standing posture (Buchanan and Horak 1999). However, vision effects in the sagittal plane remain unknown for trunk stabilization.

Perturbation bandwidths exceeding the natural frequency decrease the proprioceptive reflexive contributions in postural control of the ankle and shoulder (e.g., Stein and Kearney 1995; van der Helm et al. 2002), likely because the reflexes are unable to improve performance due to the delayed response. In neck and stance studies (Buchanan and Horak 1999; Forbes et al. 2013), high-bandwidth perturbations led to head or trunk-in-space behavior. Because the frequency range during natural movements involving the low-back is fairly low, proprioceptive reflexes may be underestimated when determined with perturbations with higher bandwidths as applied in all the above mentioned identification studies.

The goal of this study is to assess how reflexes and intrinsic properties contribute to low-back stabilization and modulate with conditions. By changing the conditions (task instruction, vision and bandwidth), changes

in the system dynamics were provoked revealing shifts in stabilization strategy. These effects were attributed to either reflexive or intrinsic muscle properties by kinematics and reflexive EMG frequency response functions and by estimating intrinsic and reflexive neuromuscular parameters.

Methods

Subjects

Six healthy young adults (age: 23–25 years, 4 male) participated in this study and gave informed consent according to the guidelines of the ethical committee of Delft University of Technology. Subjects did not experience LBP in the year prior to the experiments.

Experiments

The subjects were seated in a kneeling-seated posture (Fig. 1; 90° knee and ankle angle, 135° angle between upper body and upper legs) at a rigid chair, while being restrained at the pelvis by clamping the anterior superior and posterior iliac spine from the side. The chair was placed on top of a hydraulic hexapod motion platform, which is position-controlled through a dedicated computer system (dSpace, Paderborn, Germany) with a custom-made controller with a bandwidth up to 13 Hz (Matlab/Simulink, Mathworks Inc., Natrick, MA, USA). The seat and clamps were foam-covered for subject comfort. To avoid extra dynamics of the arms, subjects were instructed to cross their arms in front of their chest.

Upper body sway was evoked by translational platform perturbations ($P(t)$) in anterior–posterior direction. Task instructions were alternately to behave naturally (*Natural Balance task*) or to minimize flexion/extension excursions (*Resist task*). Both tasks were performed with eyes open (EO) and eyes closed (EC).

The perturbations $P(t)$ were random-appearing multisine signals of 20-s duration. Each experimental trial had duration of 80-s consisting of a 10-s fade-in period, 3 repetitions of the same perturbation signal $P(t)$, and a 10-s fade-out period. The fade-in and fade-out periods were applied to minimize transient behavior and to prevent abrupt platform motions. To investigate the effect of bandwidth on low-back stabilization, each condition was performed with three different perturbation signals, which contained 0.2 Hz as lowest frequency, while the highest frequency alternated between 1, 3, and 10 Hz (B1, B3, and B10, respectively). The excited frequencies consisted of clusters of two adjacent frequency points,

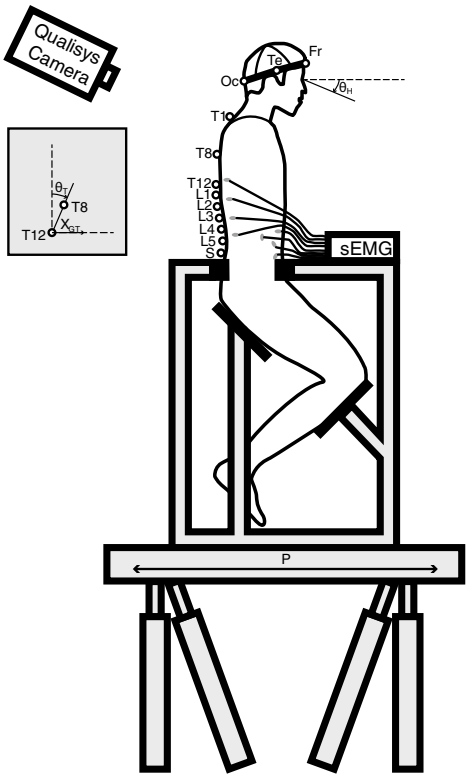

Fig. 1 Experimental setup. Markers (*open circle*) were placed on the sacrum (*S*), the lumbar vertebrae (*L1–L5*), the thoracic vertebrae (*T1*, *T8*, *T12*), the head (occipital bone (*Oc*), temple (*Te*), frontal bone (*Fr*), the left ear and the left eye socket), the acromion and the chair. Kinematics were described in platform perturbations (*P*), global trunk translations (X_{GT}), relative trunk translations ($X_{RT} = X_{GT} - P$), torso rotations (θ_T), and head rotations (θ_H). Muscle activity was measured using surface electromyography (sEMG)

which were spaced linearly (<1 Hz) and logarithmically (>1 Hz). To reduce control modulation due to high frequent perturbations, the perturbation power was reduced to 60 % above 1 Hz and 40 % above 4 Hz (Mugge et al. 2007), with flat power in velocity in these three bands (Fig. 2). To create a similar perturbation amplitude, perturbations for the three bandwidth conditions (B1, B3, and B10) were scaled toward an equal maximal acceleration power and thus perturbation force. For safety and comfort of the subjects, the maximum accelerations were kept below 1G. All 12 conditions (Table 1) were repeated twice, resulting in 24 trials per subject applied in a randomized sequence.

Data recording and processing

Three-dimensional kinematics of the low-back, trunk, and head were measured at 200 Hz using an Oqus 6-camera 3D motion capture system (Qualisys AB, Gothenburg, Sweden). Markers were placed at the sacrum, the

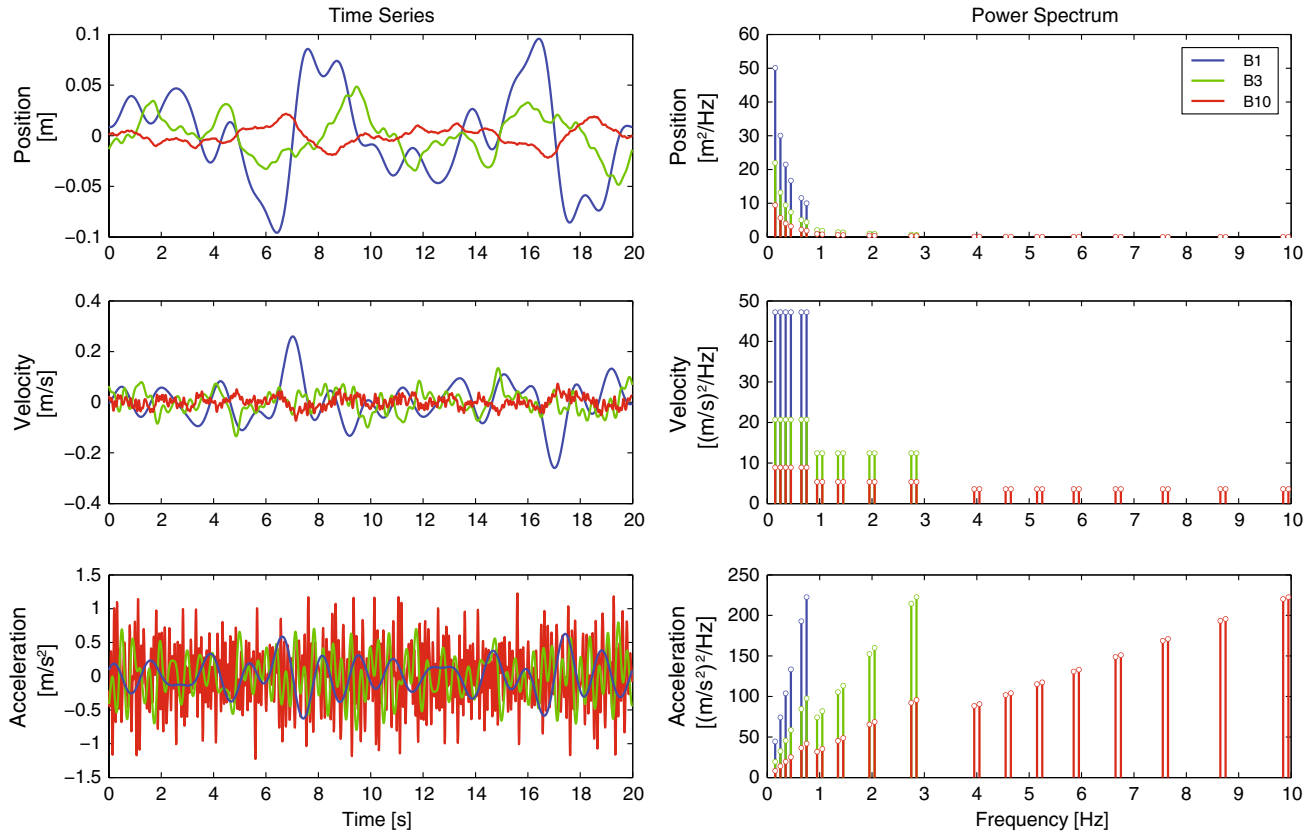

Fig. 2 Perturbation signal as time series (*left*) and power spectrum (*right*) for the perturbation bandwidths *B1* (*blue*), *B3* (*green*), and *B10* (*red*). The perturbation signal is shown as position (*top*), velocity (*middle*), and acceleration (*bottom*) signal

Table 1 Overview of the twelve experimental conditions, with the bandwidths B1 (0.2–1 Hz), B3 (0.2–3 Hz) and B10 (0.2–10 Hz), the tasks natural balance and resist, and eyes opened (EO) or closed (EC)

Perturbation	Bandwidth (Hz)	Frequency points (clusters)	Task	
			Natural balance	Resist
B1	0.15–0.75	6 (3)	EO/EC	EO/EC
B3	0.15–2.85	14 (7)	EO/EC	EO/EC
B10	0.15–9.95	30 (15)	EO/EC	EO/EC

lumbar vertebrae (L1–L5), the thorax (T1, T8, T12), the left acromion, the head (occipital bone, temple, frontal bone, anterior of the left ear in line with the tragion, and on the lower border of the left eye socket), and the chair. The global trunk translation ($X_{GT}(t)$) was based on the marker at T12. Subtracting the chair marker from X_{GT} resulted in the trunk translations relative to the platform ($X_{RT}(t)$). In the sagittal plane, the trunk rotation $\theta_T(t)$ was based on the angle of the link between the T8 and T12 markers with the vertical axis, while the head rotation $\theta_H(t)$ was obtained with the Veldpaus-algorithm (Veldpaus et al. 1988) applied to all markers on the head. Rotations occurring with flexion were considered positive.

Activity of twenty muscles (10 bilateral pairs; the back muscles m. Longissimus (at T9 and L4), m. Iliocostalis (at T12 and L2); the abdominal muscles m. Rectus Abdominus, m. Obliquus Externus (lateral and anterior), m. Obliquus internus; the hip muscles m. Gluteus Maximus and m. Rectus Femoris) was measured at 2,000 Hz [surface electromyography (sEMG); Porti 17, TMSi, the Netherlands) as described in Willigenburg et al. (2010)]. The EMG data $e_j(t)$ (with j = #muscle) were digitally filtered (zero-phase, first-order, high-pass) at 250 Hz (Staudenmann et al. 2007) and then rectified. A lumped muscle activation $E(t)$ with positive flexion activity was derived with the sixteen back and abdominal muscles by optimizing the weight factors w_j for a maximum coherence of the perturbation to EMG (Kiemel et al. 2008). Weight factors were derived per subject optimizing over all conditions:

$$E(t) = \sum_{j}^{\text{abdominal}} w_j e_j(t) - \sum_{j}^{\text{back}} w_j e_j(t),$$
$$\text{with } w_j = [0,1] \text{ and } \sum_{j}^{\text{all}} w_j = 1 \quad (1)$$

System identification

System identification techniques (Guitton et al. 1986; Pintelon and Schoukens 2001) were used to describe the low-back kinematics and reflexes as frequency response functions (FRFs). The kinematic FRFs describe the total response of the subjects including the intrinsic properties and reflexive behavior. Because torso kinematics did not influence platform perturbations, the kinematic FRFs were derived as the open-loop response to the perturbation ($P(t)$) of the global trunk translations ($X_{GT}(t)$), the relative translations of trunk ($X_{RT}(t)$) and head ($X_{RH}(t)$), and the rotations of the trunk ($\theta_T(t)$) and head ($\theta_H(t)$):

$$X(f) = \frac{S_{PX}(f)}{S_{PP}(f)}; \quad \theta(f) = \frac{S_{P\theta}(f)}{S_{PP}(f)} \quad (2)$$

with $S_{PX}(f)$ representing the estimated cross-spectral density between the Fourier-transformed signals P and X, etc.

The reflexive FRF was obtained using the joint input–output approach (van der Kooij et al. 2005), which uses an external perturbation to identify the closed-loop response of lumped EMG ($E(t)$) to the trunk flexion/extension angle ($\theta_T(t)$):

$$E(f) = \frac{S_{PE}(f)}{S_{P\theta_T}(f)} \quad (3)$$

The cross-spectral densities were only evaluated at the frequencies containing power in the perturbation signal. For improved estimates and noise reduction, the cross-spectral densities were averaged across the six time segments per condition and over two adjacent frequency points (Jenkins and Watts 1969). Coherence was calculated to evaluate input–output relationship:

$$\gamma_X^2(f) = \frac{|S_{PX}(f)|^2}{S_{PP}(f)S_{XX}(f)}; \quad \gamma_\theta^2(f) = \frac{|S_{P\theta}(f)|^2}{S_{PP}(f)S_{\theta\theta}(f)};$$
$$\gamma_E^2(f) = \frac{|S_{PE}(f)|^2}{S_{PP}(f)S_{EE}(f)} \quad (4)$$

Coherence ranges from 0 to 1, where one reflects a perfect, noise-free relation. Since spectral densities were averaged over 12 points, coherence greater than 0.24 is significant with $p < 0.05$ (Halliday et al. 1995).

Physiological modeling

A linear neuromuscular control (NMC) model was constructed to describe the lumbar stabilization with physiological elements of intrinsic and reflexive contributions (Fig. 3). This model represents an inverted pendulum with one degree of freedom, describing the kinematic trunk rotations $\theta_T(t)$ and the EMG $E(t)$. The virtual pivot point was determined for each subject using the recorded T12 kinematics dividing $X_{RT}(f)$ by $\theta_T(f)$ (see results and Fig. 6). The effective mass (m) and center of mass of the upper body were defined anthropometrically (Clauser et al. 1969) resulting in an average mass of 37.3 ± 4.8 kg located at a height (h) 296 ± 20 mm above the virtual pivot point. The intrinsic elements lump passive tissue properties, muscle co-contraction, cross-bridge dynamics, and force–length and force–velocity relationship into two parameters describing the overall lumbar stiffness and damping (k, b). The reflexive contribution is a combination of spindle modulation, tonic drive and presynaptic inhibition described by a position and a velocity feedback gain (k_p, k_v) with a time delay (τ_{ref}). Second-order muscle activation dynamics were implemented (Bobet and Norman 1990) with a cutoff frequency (f_{act}) and a dimensionless damping factor (d_{act}). To translate the reflexive forces to EMG in mV, a scaling parameter (e_{scale}) was included. For eyes-open conditions, visual feedback was included as an additional position feedback (k_{vis}) with a long-latency time delay (τ_{vis}) of 250 ms (Goodworth and Peterka 2009).

The parameters were identified by fitting the NMC model on the FRFs of both the low-back kinematics and the reflexive muscle activation for all repetitions. All conditions were optimized simultaneously assuming the time delays, activation dynamics, and EMG scaling to be constant over all conditions within subjects. The criterion function used in the estimation was:

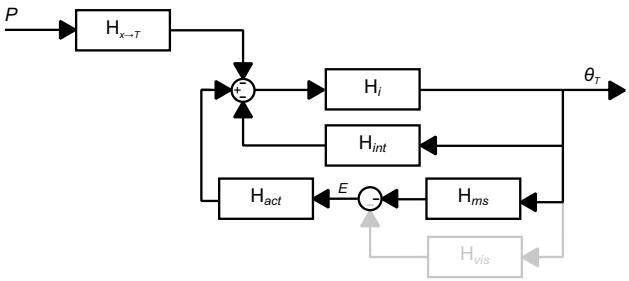

Fig. 3 Physiological model. The input perturbation (P) was applied as platform translation and resulted in trunk rotation (θ_T) and EMG activity (E). Involved are the dynamics of the trunk inertia in the presence of gravity ($H_i = 1/(mh^2s^2 - mgh)$) and intrinsic properties ($H_{int} = bs + k$). Reflexive feedback is described by muscle spindle ($H_{ms} = (k_v s + k_p)\, e^{-\tau ref\, s}$) and visual feedback ($H_{vis} = k_{p,vis}\, e^{-\tau vis\, s}$). The platform translational perturbations were transformed into low-back torques ($H_{x\to T} = mhs^2$). This results in the overall transfer functions of the modeled trunk rotations ($\theta_{mdl}(f) = -H_{x\to T} / (H_i^{-1} + H_{int} + (H_{ms} + H_{vis})\, H_{act})$) and EMG activity ($E_{mdl}(f) = -H_{ms}$). The visual feedback was applied for the eyes-open conditions only

$$\text{err} = \sum_{1}^{\#\text{rep}} \sum_{k} \frac{\gamma_{\theta}^{2}(f_k)^2}{1+f_k} \left| \log \left(\frac{\theta_{\text{T}}(f_k)}{\theta_{\text{mdl}}(f_k)} \right) \right|^2 + q^2 \sum_{1}^{\#\text{rep}} \sum_{k} \frac{\gamma_{E}^{2}(f_k)^2}{1+f_k} \left| \log \left(\frac{E(f_k)}{E_{\text{mdl}}(f_k)} \right) \right|^2 \quad (5)$$

with f_k as the power-containing frequencies, and θ_{mdl} and E_{mdl} as the kinematic and reflexive transfer functions of the model. To provide equal contributions of the kinematics and reflexive muscle activity to the criterion function, a scaling factor q of 0.75 was used.

The validity of the optimized model and its parameters was assessed in the time domain using the variance accounted for (VAF). A VAF of 1 reflects a perfect description of the measured signal by the model. The experimental measurements of $\theta(t)$ were compared with the estimated model outcomes $\theta_{\text{mdl}}(t)$:

$$\text{VAF}_{\theta} = 1 - \frac{\sum_{1}^{n} (\theta(t_n) - \theta_{\text{mdl}}(t_n))^2}{\sum_{1}^{n} (\theta(t_n))^2} \quad (6)$$

with n as the number of data points in the time signal. For the EMG, VAF_E was calculated by replacing $\theta(t)$ and $\theta_{\text{mdl}}(t)$ with $E(t)$ and $E_{\text{mdl}}(t)$, respectively. To reduce noise contributions, measured data were reconstructed with only the frequencies that contain power in the perturbation.

The accuracy of the parameters was evaluated by the standard error of the mean (SEM) (Ljung 1999):

$$\text{SEM} = \frac{1}{N} \text{diag} \left[\left(J^T J \right)^{-1} \right] \sum \text{err}^2 \quad (7)$$

where the Jacobian J contains the gradient of the predicted error err to the optimal parameter vector. The SEM was defined as the percentage of the subject-averaged parameter values. The more the influence a parameter has on the optimization criterion, the smaller the SEM will be.

Statistics

A parametric linear mixed model was applied to assess the effect of vision, bandwidth, and task instruction. The statistical model took into account the main and the two-way interaction effects of the different conditions. Statistics were performed on the averaged gain and phase of the FRFs at the lowest frequency points (Fig. 5) and the parameters of the model (Fig. 8). A Bonferroni-corrected p value smaller than 0.05 was considered significant.

Results

Frequency response functions (FRFs)

Human low-back stabilizing behavior for the highest bandwidth (0.2–10 Hz) is described by the FRFs of the kinematics and EMG (Fig. 4). Kinematics are described in global trunk translations ($X_{\text{GT}}(f)$), trunk and head translations relative to the platform ($X_{\text{RT}}(f)$ and $X_{\text{RH}}(f)$), and trunk and head rotations ($\theta_T(f)$ and $\theta_H(f)$). The lumped EMG ($E(t)$) constructed out of back and abdominal muscles had the m. Longissimus at L4 level (26 %), m. Rectus Abdominus (19 %), and lateral m. Oblique Externus (16 %) as main contributors (see Table 2 in the Appendix). The EMG response ($E(f)$) is described relative to the trunk rotations. All conditions have coinciding FRFs above 3 Hz, while systematic effects of vision, task, and bandwidth on gain and phase were found below 1 Hz. These effects of vision, task, and perturbation bandwidth below 1 Hz are shown in Fig. 5 after averaging over the six lowest measured frequency points.

High coherences (>0.8) were found for the kinematics and EMG above 0.7 Hz, indicating good input–output correlation. Below 0.7 Hz, lower coherences (except for X_{GT}) indicate movements unrelated to the perturbation, including natural postural sway. Measurement of a marker at the sacrum showed that platform translations were well transmitted to the sacrum below 5 Hz, while above 5 Hz, sacrum motion showed some amplification with phase lag, which contributes to the inaccuracy of the model at the highest frequencies.

The FRFs of X_{RT} and θ_T were very similar in shape (Figs. 4, 5). Up to 5 Hz, the trunk kinematics could be well described with a virtual rotation point located between vertebrae L4 and L5 (on average 138 mm below T12; Fig. 6). Above 5 Hz, more complex dynamics were apparent resulting in dissimilar X_{RT} and θ_T FRFs and a lower virtual rotation point suggesting S-shape low-back bending.

The trunk rotation FRF (θ_{T}) resembles the characteristics of a second-order system with a natural frequency around 1 Hz. Below the natural frequency, a gain slope between +1 and +2 was found, indicating dominant behavior of the intrinsic stiffness (represented by a gain slope of +2), damping (gain slope of +1), and reflexes (gain slope between +2 and +1, depending on the type of reflex). Above the natural frequency, inertia is dominant indicated by a flat gain. The EMG FRF (E) shows a gain slope between 0 and +1 up to approximately 5 Hz, indicating a combination of position (flat gain, −180° phase) and velocity (+1 gain slope, −90° phase) feedback. At higher frequencies, an additional acceleration/force feedback (slope of +2 in gain, 0° phase) in combination with a phase decrease due to reflex delays seems present.

The kinematic FRFs can be interpreted as trunk-in-space (the trunk perfectly stationary in space; X_{GT}: gain of 0; X_{RT}: gain and phase of 1° and −180°; θ_T: phase of −180°) or trunk-on-pelvis (the trunk moving perfectly in line with the pelvis; X_{GT}: gain and phase of 1° and 0°). Trunk-on-pelvis behavior was observed up to ~1 Hz and resulted in 8–32 % relative

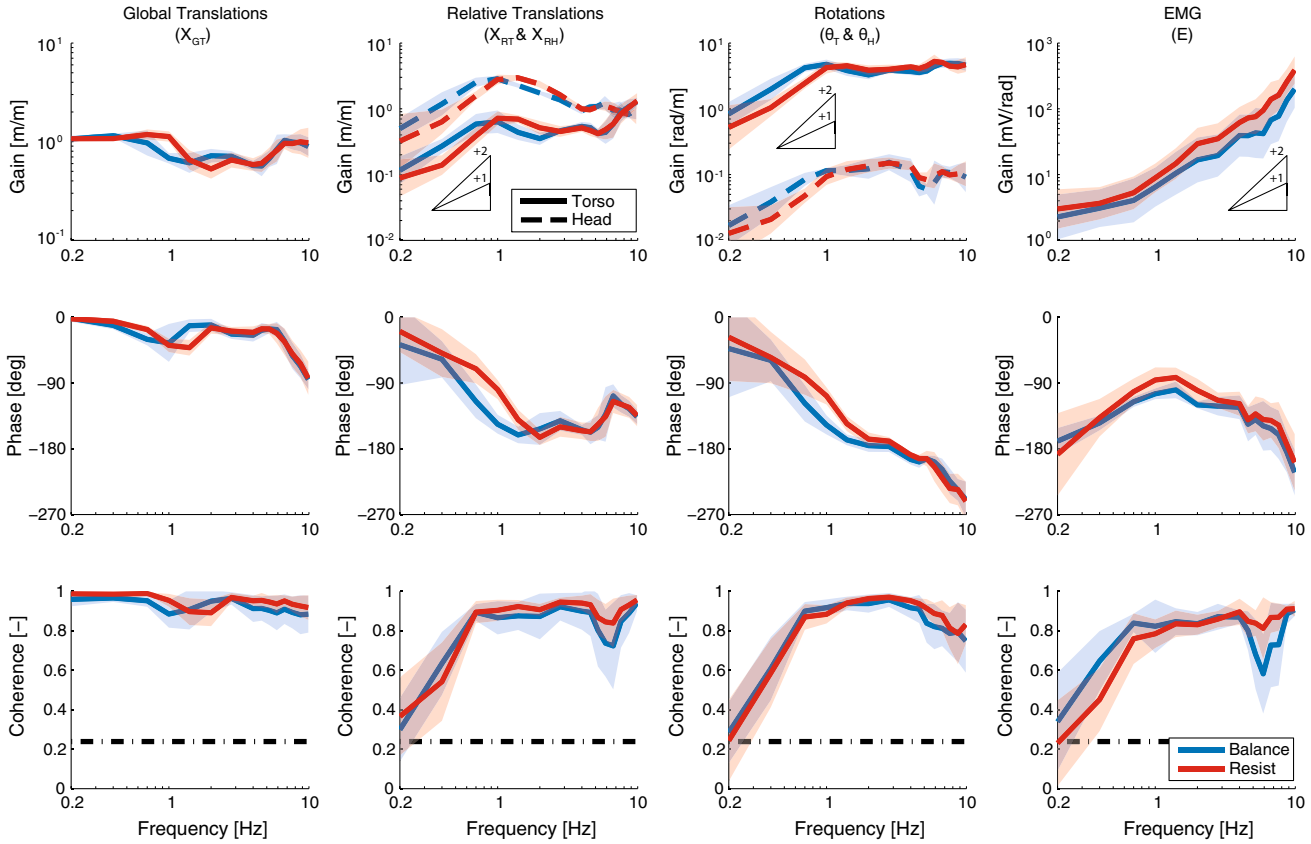

Fig. 4 FRFs of the trunk (*solid*) and head (*dashed*) kinematics and EMG during the 10-Hz perturbations and the eyes-closed condition. The kinematics are described by the global translations in space (X_{GT}), the translations relative to the pelvis (X_{RT} and X_{RH}), and rotations in space (θ_T and θ_H). The gain (amplitude difference), phase (time shift), and coherence (correlation) illustrate the transformation of the input signal into the output signal. The different colors represent the natural balance (*blue*) and the resist (*red*) task. The *triangles* are given as reference to the slope of the gains indicating stiffness (+2), damping (+1) and mass (0) in the relative translations and rotations and position feedback (0), velocity feedback (+1) and acceleration, and/or force feedback (+2) in the EMG. The FRF average (*lines*) and standard deviation (*shades*) over subjects are shown

trunk translations (see Figs. 4, 5). Between 1 and 5 Hz, trunk kinematics shifted to trunk-in-space (X_{RT}: gain between 0.5 and 1 and phase of −180°), reducing X_{GT} by 40 %.

The head showed a stationary orientation behavior, with head rotations θ_H only ~2 % of the trunk rotations θ_T displaying a similar shape of gain with head rotations lagging behind trunk rotations at higher frequencies. The relative head translations (X_{RH}) were ~4 times larger than the trunk (X_{RT}) with a similar shape of gain and phase lag. Up to 3 Hz, the global head translations (X_{GH}) exceeded global trunk translations (X_{GT}) with 20 % (see Fig. 10 in the Appendix).

Physiological modeling

Figure 7 illustrates that the model adequately fits kinematics (below 5 Hz) and EMG for the 10-Hz bandwidth condition with EC, while VAF values for all conditions (Fig. 8) show reasonable to good time domain fits ($VAF_\theta = 78$ %; $VAF_e = 65$ % averaged over all conditions and subjects). Above 5 Hz, the single degree of freedom model was unable to describe the more complex kinematic behavior as described above. This did not influence the accuracy of the intrinsic and reflexive parameters estimates (Fig. 8) as confirmed by an average SEM of 46 %, because these parameters are predominantly involved in the kinematic response below 5 Hz. Models incorporating vestibular and visual feedback were explored, but resulted in inaccurate parameter estimates. Because the linear model was unable to describe uncorrelated data as described by low coherencies (see Fig. 4), the lowest frequency (0.2 Hz) was excluded from modeling.

For static model stability, the effective stiffness (combined intrinsic stiffness and position feedback) was bounded to be equal or higher than the negative proportional effect of gravity. The effective stiffness was dominated by the intrinsic stiffness (92 % averaged over all conditions), while the estimated MS position feedback

even became negative for several conditions. The effective damping was separated into MS velocity feedback (61 %) and intrinsic damping.

Effects of vision, task instruction, and perturbation bandwidth

In Fig. 5, the effects of bandwidth, vision, and task instructions are shown for gain and phase below the low-back natural frequency (1 Hz). As shown for task effect (Fig. 4) and vision (Fig. 7), FRFs were not different between conditions above 3 Hz. The intrinsic and reflexive model parameters are shown in Fig. 8.

Effect of vision

Significant vision effects were found in kinematic and EMG FRFs and in the modeling results. The gain of X_{GT} decreased ($p < 0.001$) and became smaller than one with eyes open, indicating a tendency toward trunk-in-space behavior. This was obtained by moving more in opposite direction of the platform (θ_T: phase of $-180°$), as described by the phase decrease of approximately $-40°$ ($p < 0.001$) in θ_T. In line with the trunk-in-space behavior, the decrease in gain of the EMG ($p < 0.05$) and reflexive gains [k_p ($p < 0.001$), k_v ($p < 0.02$)] resulted in higher compliance. Surprisingly, the relative trunk motions during the EO condition were smaller than during the EC condition [decreased gain of θ_T ($p < 0.02$) during EO], indicating a better performance for both trunk-on-pelvis and trunk-in-space stabilization with the eyes open.

The effective stiffness ($k + k_p$) exceeded the gravitational negative stiffness only marginally (+1 %) during the EO conditions. During the EC conditions, the effective stiffness increased substantially (+14 %), resulting in a larger stability margin.

The model could not well describe the kinematic phase below $-90°$ at the lowest frequencies during EO conditions (Fig. 7), which led to slightly lower VAF values (Fig. 8). As an exploration, an additional visual feedback loop was included in the model with long-latency (250 ms) position feedback (see Fig. 3), improving the fit of the kinematic

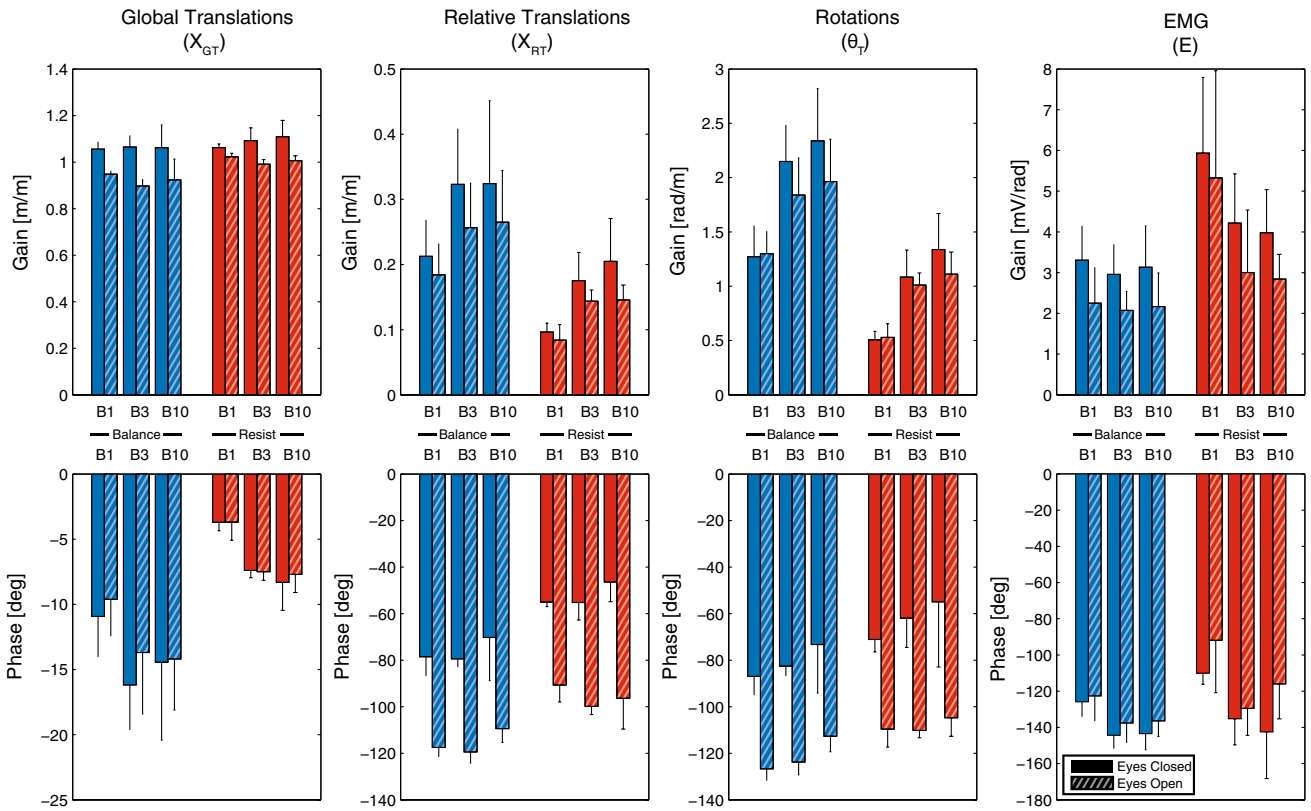

Fig. 5 Kinematics and EMG modulation due to task instruction (natural balance and resist), bandwidth (B1, B3 and B10), and vision (eyes closed (*solid*) and open (*striped*)). Gains and phases were averaged over the low frequencies (<1 Hz). Values are the mean (*bars*) and standard deviations (*error bars*) over subjects. A lower X_{GT} gain and a larger phase lag for X_{RT} and θ_T describes modulation toward trunk-in-space stabilization. Modulation toward trunk-on-pelvis is illustrated by a X_{GT} closer to 1 (gain) and 0° (phase) and smaller gains for X_{RT} and θ_T. The results indicate modulation toward trunk-in-space stabilization with eyes open, the balance task and increasing bandwidths

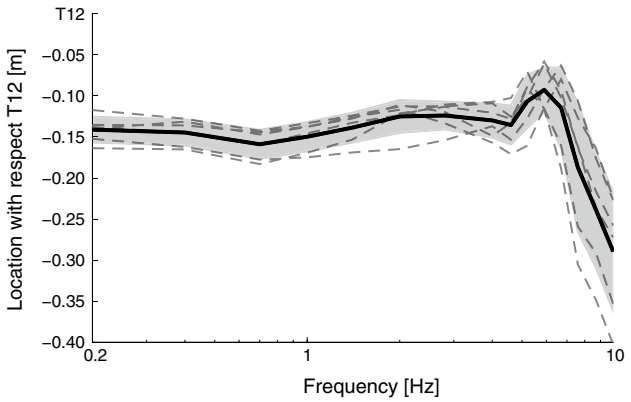

Fig. 6 Lumbar virtual rotation point location below T12. The vertical position is derived for each frequency by dividing $X_{RT}(f)$ by $\theta_T(f)$ averaged over all conditions. The lumbar virtual rotation point is shown for separate subjects (*dotted lines*) and averaged over subjects (*solid line with shadow* as standard deviation). Results illustrate that a fixed rotation point (−138 mm with respect to T12) located between L4 (−123 mm) and L5 (−151 mm) adequately captures lumbar bending up to 5 Hz. The deviation of the lumbar virtual rotation point above 5 Hz suggests higher order dynamics such as S-shape bending

phase and the EMG (Fig. 7) and increasing both VAF_θ and VAF_e with ~5 %. However, high SEM values indicated poor parameter estimates.

Effect of task instruction

The task instruction to resist led to a 49 % reduction of θ_T below 1 Hz ($p < 0.001$) with respect to the natural balance task, indicating a shift to trunk-on-pelvis behavior. Between 1 and 2 Hz, the gain of θ_T increased for the resist task, indicating a trade-off for better task performance at the lower frequencies. The additional resistance was achieved by increased co-contraction (increased RMS_{EMG} of 30 % ($p < 0.02$) and higher intrinsic stiffness ($p < 0.007$) and damping ($p < 0.001$)) and reflex gains (increased EMG gain of 104 % ($p < 0.002$), and increased k_v ($p < 0.001$)).

Effect of perturbation bandwidth

Significant bandwidth effects were found comparing bandwidth B1 on one hand and bandwidths B3 and B10 on the other hand, while between B3 and B10, no significant differences were found. For B3 and B10, the gain of θ_T increased significantly ($p < 0.001$), indicating a less active trunk-on-pelvis stabilization. This was mainly attributed to a 65 % decrease in intrinsic damping ($p < 0.001$). Interestingly, there was no significant change of the intrinsic stiffness and RMS_{EMG}, ruling out decreased co-contraction. The larger phase lag of the EMG ($p < 0.001$) indicates reflex modulation with a reduced role of velocity feedback, which was described by a small increase in k_p ($p < 0.04$).

Discussion

The goal of this study was to assess reflexive and co-contractive contributions to low-back stabilization and motor control modulation with changed conditions. Upper body sway was evoked by anterior–posterior platform translations, while subjects were seated with the upper body free and the pelvis restrained. Kinematic and reflexive frequency response functions (FRFs) and physiological model parameters were obtained describing low-back motor control. Substantial motor control modulations were observed for all varying conditions (vision, task instruction, and perturbation bandwidth) in particular at the lowest frequencies (<1 Hz).

The main objective of low-back stabilization is to keep the trunk posture upright, while counteracting gravity. To achieve this, the effective stiffness (intrinsic stiffness and reflexive feedback combined) should exceed the gravitational negative stiffness, resulting in a positive net stiffness. In whole-body postural control experiments, a net stiffness close to zero was observed (Loram and Lakie 2002; van der Kooij et al. 2004). This minimizes effort and is closely related to a trunk-in-space strategy, in which just-sufficient low-back stiffness neutralizes the transfer of pelvic perturbations to the trunk. This stabilization strategy was found in this study during EO conditions, expressed by the slope of +1 in the trunk rotation FRF and an effective stiffness of only 101 % of the destabilizing gravitational component.

Effect of vision

The EO conditions tended to trunk-in-space behavior, which was described by a greater phase lag in θ_T and a X_{GT} gain smaller than 1. Similar observations were found in whole-body and head–neck posture control (Buchanan and Horak 1999; Forbes et al. 2013). The trunk-in-space behavior was obtained by decreased reflexes, which is consistent with whole-body postural control experiments (Collins and De Luca 1995; van der Kooij et al. 2004). During the EC conditions, a trunk-on-pelvis behavior was achieved by increased effective stiffness (114 % of negative gravitational stiffness), indicating a strategy with a larger stability margin and higher effort. Surprisingly, however, the EC conditions led to more low-back motions (θ_T gain increased), and therefore worse trunk-on-pelvis stabilization. An explanation could be that the higher effective stiffness led to more movement of the center of mass and therefore higher inertial forces due to the perturbation.

During EO conditions, the model could not well describe the kinematic phase below −90° at the lowest frequencies (see Fig. 7), which led to slightly lower VAF values. This indicates that vision does not only modulate

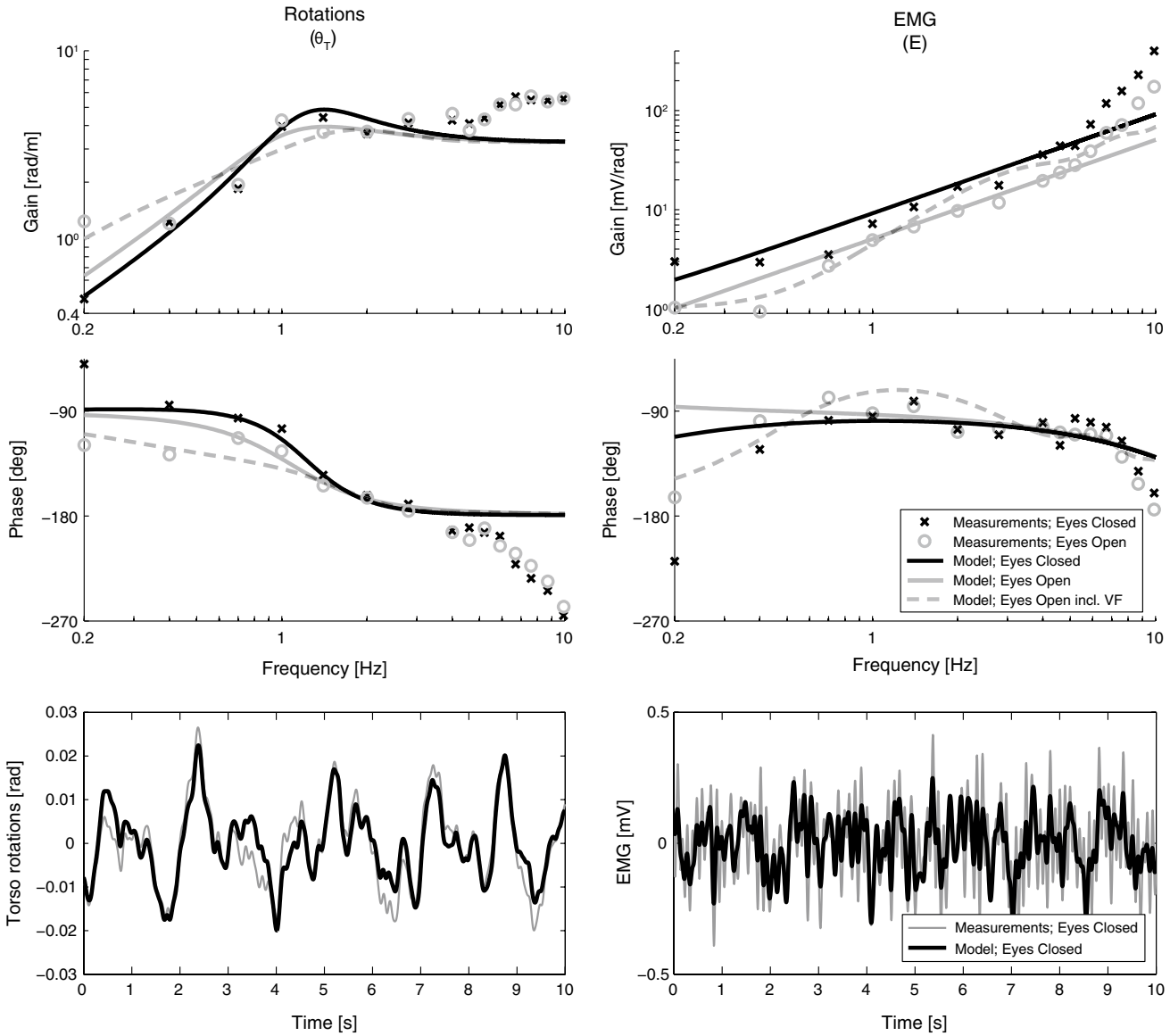

Fig. 7 Example of the model fit of the torso rotations (*left*) and the EMG (*right*). Results are representative for all conditions. *Top* FRF model fit for the resist task during 10-Hz perturbation bandwidth with EO (*gray*) and EC (*black*). Crosses and circles represent measured data. Solid lines show fits using the standard model. *Dotted lines* show fits using an explorative model with an additional visual feedback loop effecting mainly low-frequent modeling results. *Bottom* Time domain model fit (*black line*) and measurements (*gray*, *dotted line*) for the resist task during 10-Hz perturbation bandwidth and EC conditions

the proprioceptive reflexes and intrinsic properties, but also provides extra information. Direct visual feedback contributes only at low frequencies (Berthoz et al. 1978), because of the visual processing time which results in a long-latency time delay (>200 ms). As an exploration, a long-latency (250 ms) position feedback was included in the model representing the visual contribution (Goodworth and Peterka 2009). With 0.2 Hz as lowest measured frequency point, the data did not contain enough information to estimate the gain (and time delay) of such a long-latency feedback loop properly. However, the model with direct visual feedback described the kinematic phase and EMG better at the lowest frequencies (Fig. 7) and led to a 5 % increase in both the VAF_{θ} and the VAF_{e} during eyes-open conditions. This indicates that position feedback directly contributes to lumbar stabilization, but separate perturbations of the visual field are needed to accurately estimate the visual feedback parameters.

Effect of task instruction

The resist task demanded a trunk-on-pelvis stabilization strategy, which was observed as reduced low-back motions (θ_T gains) at the lowest frequencies. This modulation led

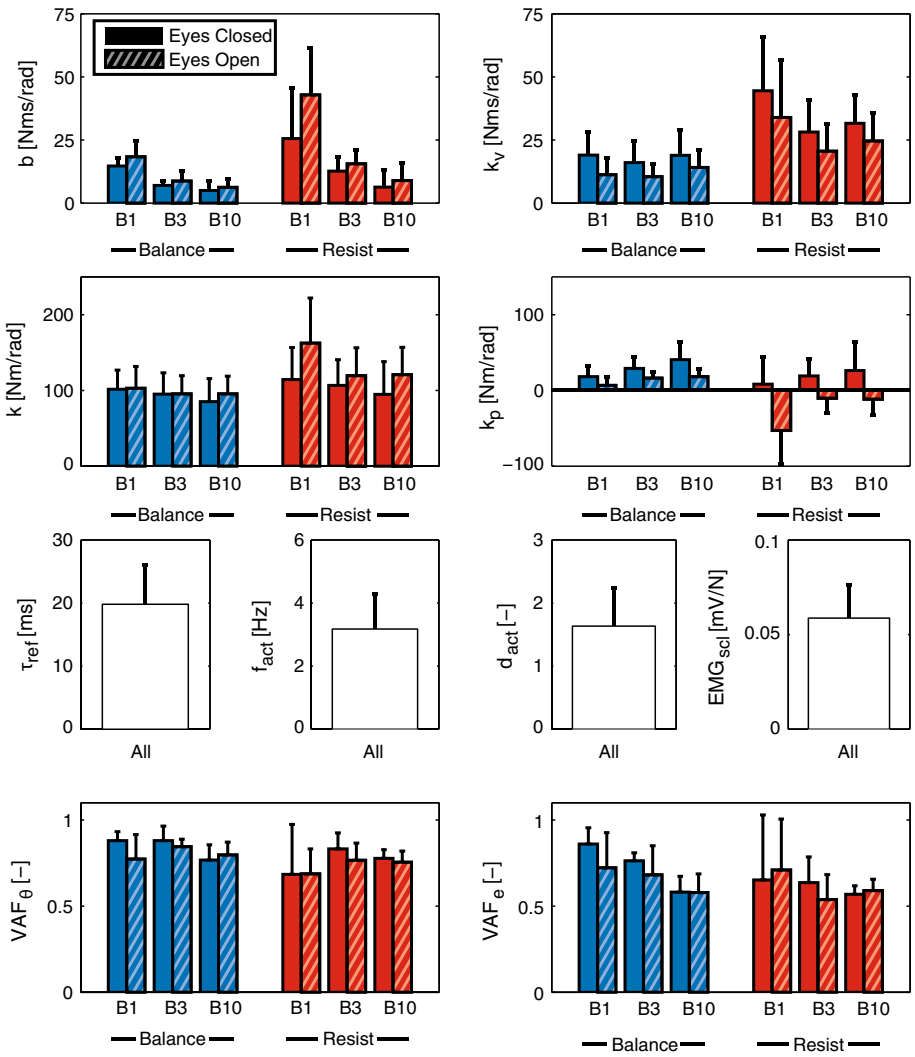

Fig. 8 Parameter values and VAFs of the kinematics and EMG (VAF_θ and VAF_e) for all conditions. Values are the mean (*bars*) and standard deviation (*error bars*) over all subjects

to higher θ_T gains around the natural frequency (1–2 Hz). These effects of task are similar in direction, but smaller in magnitude than in previous experiments applying a trunk perturbation force at the back (van Drunen et al. 2013). This could be explained by the perturbation type. In contrast to trunk perturbations, pelvis perturbations are not applied directly on the effective trunk mass. The higher stiffness and damping during the resist task will result in more motion of the center of mass and thus larger inertial torques.

The modulation with task was attributed to higher co-contraction levels (higher RMS_{EMG} and intrinsic stiffness and damping) and higher reflexive velocity feedback. Different to the trunk perturbation experiments was the decrease in reflexive position feedback during the resist task, which was most dominant during EO conditions with even negative estimated k_p values. This may represent an effort to decrease the (perturbation) torques by maintaining a constant effective stiffness and therefore compensating for the increased intrinsic stiffness.

Effect of perturbation bandwidth

Significant differences in low-back motor control were found between bandwidth B1 below the low-back natural frequency (~1 Hz) and B3 and B10 exceeding the natural frequency, while no differences were found between B3 and B10. Trunk-on-pelvis performance became worse with high perturbation bandwidths, which was attributed to a decrease in intrinsic damping and slight increase in position feedback. Because the intrinsic stiffness and RMS_{EMG} were unaltered, the modulation in the intrinsic damping was not part of decreasing co-contraction levels, suggesting nonlinear muscle dynamics (e.g., force–velocity relationship, cross-bridge dynamics). This indicates that bandwidth effects should not be ignored and that motor control estimated with high-bandwidth perturbations do not fully represent the intrinsic and reflexive behavior during most (low-bandwidth) daily life activities.

Bandwidth effects are often related to reduced reflexive gains when perturbations exceed the natural frequency, because high reflex gains induce resonance peaks caused by the reflexive delay (e.g., Stein and Kearney 1995; van der Helm et al. 2002). In contrast to this theory, modeling results showed a lower resonance peak during the B1 condition. This result in combination with the slightly increased position feedback does not support this theory for low-back stabilization.

In this study, the perturbation signals with different bandwidth were scaled to achieve the same maximal acceleration power and thus perturbation force, resulting in less power in the lowest frequencies for the high-bandwidth perturbations (see Fig. 2). This scaling resulted in a similar perceived perturbation severity, but there is a possibility that the scaling also affected the modulation.

Head kinematics

Head stabilization in space enhances visual perception and motion-related comfort. Visual and vestibular feedback pathways act to stabilize the head orientation and position in space (Day 1997; Goodworth and Peterka 2009), controlling muscles in the neck and other relevant body parts. Results showed that head orientation was effectively minimized by the neck, as only 2 % of the trunk rotations (θ_T) were reflected in the head rotations (θ_H). The same is not applicable to global head position, where the global head translations (X_{GH}) exceed the global trunk translations (X_{GT}) by 20 %. Furthermore, ~4 times larger relative translations (with similar phase) were observed for the head (X_{RH}) than for the trunk (X_{RT}) consistent with movement of an inverted pendulum [for reference; relative translations of T1 being the base of the neck were approximately 3 times larger as T12 (X_{RT})]. Apparently, the neck does not compensate (by complex (S-shaped) neck bending) for the head translations resulting from platform motion and lumbar bending. This indicates that low-back motor control is involved in head-in-space stabilization and could explain the low-back motor control modulations due to vision.

Limitations and future directions

The applied system identification approach assumes linear, time-invariant behavior. Therefore, the experimental conditions were designed to evoke only small deviations around a single working point (to minimize nonlinear behavior) during a short period of time (to minimize time-variant behavior).

The surface EMG only measured superficial low-back muscles, while also deep low-back muscles are expected to play a role in low-back stabilization. By using

Table 2 The resulting weighting factors (wj [%]) describing the contribution to the lumped EMG signal of all individual muscles [the Longissimus muscle at trunk (LT) and lumbar (LL) level, the Iliocostalis Muscle at trunk (IT) and lumbar (IL) level, the Rectus Abdominus muscle (RA), the Oblique Externus muscle anteriorly (OEA) and laterally (OEL) and the Oblique Internus muscle (IO)]. Contribution was separated in the left (l) and right (r) side muscles. For better overview, all values <1 % were omitted

	Subjects						Mean
	1	2	3	4	5	6	
Back muscles							
LTr	9.9	9.9		7.8	4.8	8.2	6.8
LTl	4.7			5.6	7.5	13.9	5.3
ITr		1.1	5.6		3.5		1.7
ITl	2.7	5.6	8.7	6.1			3.9
ILr		14.2		4.4	5.3	1.5	4.2
ILl	1.7	3.0	11.4	12.3	6.4	2.7	6.3
LLr	26.6	15.1	8.1	16.6	16.6	12.4	15.9
LLl	12.1	5.7	3.3	6.6	16.4	16.1	10.0
Abdominal muscles							
RAr	12.3	17.4		18.0	5.0	10.1	10.5
RAl	7.9	11.4	3.3	13.4		13.2	8.2
IOr	4.2		1.8				1.0
IOl		2.0	7.8				1.7
OEAr		9.1	12.8		4.5		4.5
OEAl	4.9	2.3	1.6	4.8	4.9	6.8	4.2
OELr	4.7	1.6	14.0	2.4	13.5		6.0
OELl	7.1	1.6	21.5	1.7	11.6	15.0	9.8

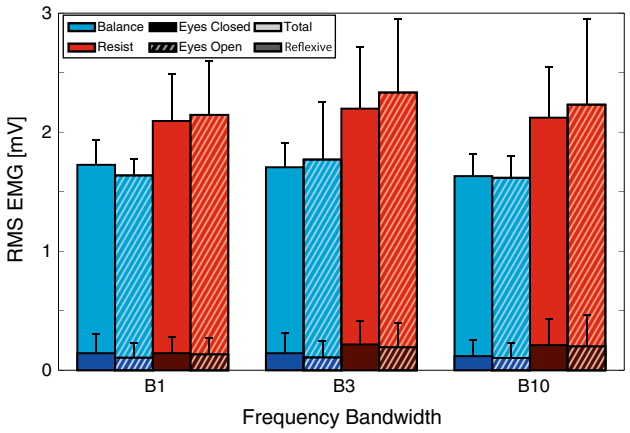

Fig. 9 Subject-averaged root mean square (RMS) of the EMG during all conditions. The total RMS (*light*) includes co-contraction and reflexive contribution, while the reflexive EMG is described by the RMS of the EMG signal with only the perturbed frequencies (*dark*)

intramuscular EMG, the role of both superficial and deep low-back muscles could be assessed.

Low-back motor control involves multiple joints, muscles and sensory systems (such as proprioceptive, cutaneous, vestibular and visual information). Kinematic analysis of a virtual low-back rotation point (Fig. 5) justified the simplification into a single inverted pendulum up to 5 Hz, while a higher order dynamic system could improve modeling results above 5 Hz. On top of that, inclusion of vestibular, visual, and Golgi tendon organ (GTO) feedback was explored in this study, but did not lead to accurate parameter estimates indicating that the data did not contain enough information to estimate their separate contributions. Perturbing a specific sensor (with e.g., visual field perturbations, galvanic vestibular stimulation (GVS)) can further quantify the contribution of these feedback systems to low-back stabilization.

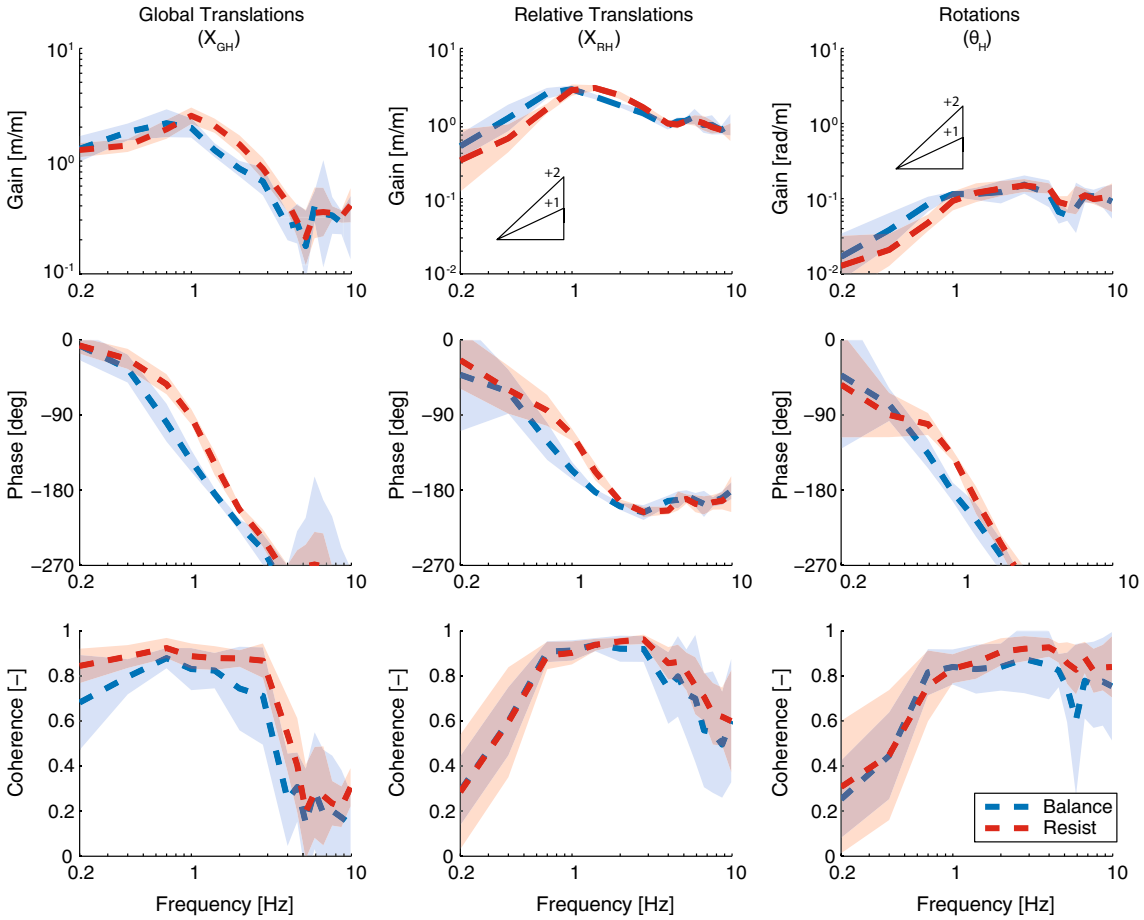

Fig. 10 FRFs of the head kinematics and EMG during the 10-Hz perturbations and the eyes-closed condition. The head kinematics are described by the global translations in space (X_{GH}), the translations relative to the pelvis (X_{RH}) and rotations in space (θ_H). The gain (amplitude difference), phase (time shift) and coherence (correlation) illustrate the transformation of the input signal into the output signal. The *different colors* represent the natural balance (*blue*) and the resist (*red*) task. The *triangles* are given as reference to the slope of the gains indicating stiffness (+2), damping (+1) and mass (0) in the relative translations and rotations and position feedback (0), velocity feedback (+1) and acceleration, and/or force feedback (+2) in the EMG. This is Fig. 4 but for head kinematics

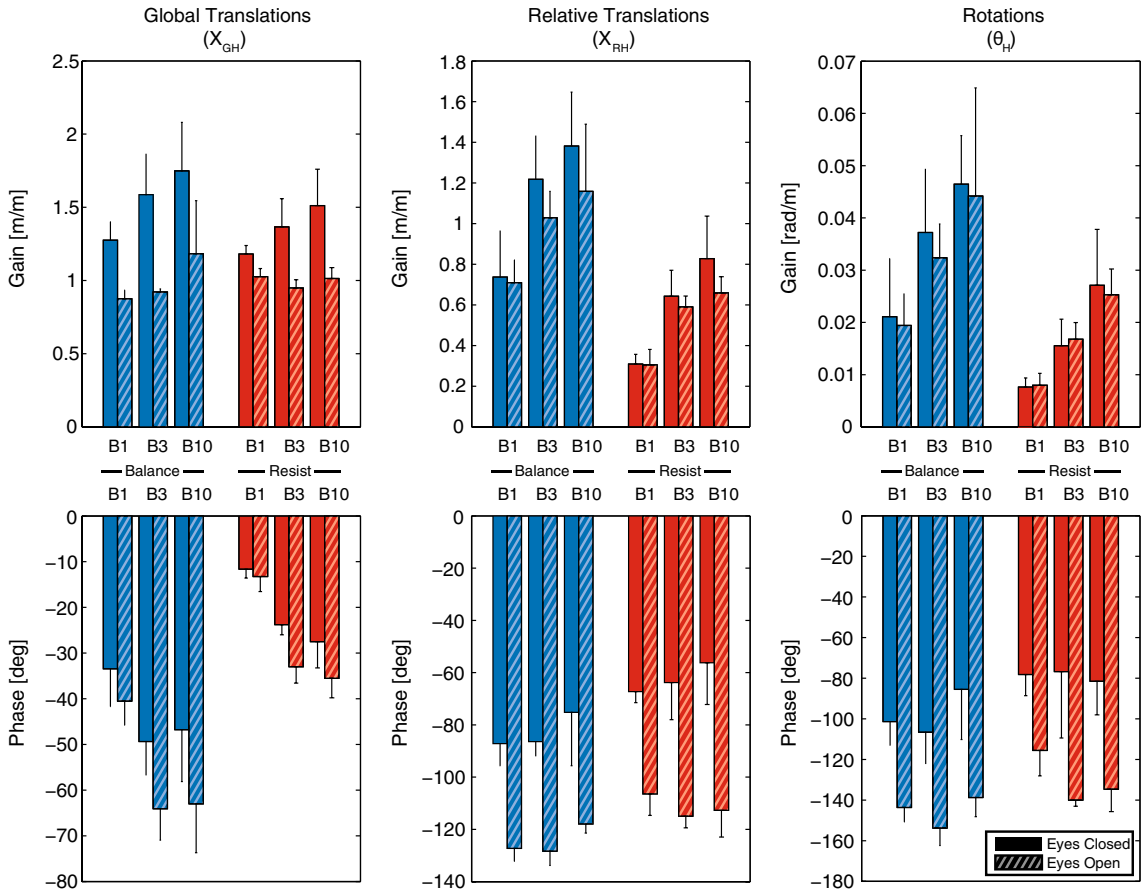

Fig. 11 Kinematics and EMG modulation due to task instruction (balance and resist), bandwidth (B1, B3 and B10), and vision (eyes closed (*solid*) and open (*striped*)). Gains and phases were averaged over the low frequencies (<1 Hz). Values are the mean and standard deviations over subjects. A lower X_{GH}-gain and a larger phase lag for X_{RH} and θ_H describes modulation toward head-in-space stabilization. Modulation toward head-on-pelvis is illustrated by a X_{GH} closer to 1 (gain) and 0° (phase) and smaller gains for X_{RH} and θ_H. This is Fig. 5 but for head kinematics

Finally, this study identified intrinsic and reflexive contribution to low-back stabilization in healthy subjects and how vision, task instruction, and bandwidth resulted in modulation of the low-back motor control. These methods can be applied on low-back pain patients to identify possible deficits in low-back motor control and its modulation.

Conclusions

- Low-back motor control modulation was found with conditions varying in vision (eyes open and closed), task instruction (natural balance and resist), and perturbation bandwidth (from 0.2 up to 1, 3, and 10 Hz) during anterior–posterior translational pelvis perturbations with a free upper body.
- Stabilization strategies were altered resulting in modulation of intrinsic stiffness and damping and proprioceptive feedback gains.
- Eyes open led to a modulation toward a trunk-in-space strategy, with direct (long-latency) visual feedback and reduced proprioceptive feedback.
- A task instruction to resist led to a modulation toward a trunk-on-pelvis strategy, which was achieved by higher co-contraction levels and increased reflexive velocity feedback.
- Perturbations with a bandwidth below the low-back natural frequency (~1 Hz) led to better performance on the trunk-on-pelvis strategy.

Acknowledgments This research is supported by the Dutch Technology Foundation STW, which is part of the Netherlands Organization for Scientific Research (NWO), and which is partly funded by the Ministry of Economic Affairs. See www.neurosipe.nl—Project 10732: QDISC.

Appendix

See Table 2 and Figs. 9, 10 and 11.

References

Berthoz A, Lacour M, Soechting J, Vidal P (1978) The role of vision in the control of posture during linear motion. Prog Brain Res 50:197–209

Bobet J, Norman RW (1990) Least-squares identification of the dynamic relation between the electromyogram and joint moment. J Biomech 23:1275–1276. doi:10.1016/0021-9290(90)90386-h

Brown SHM, McGill SM (2008) Co-activation alters the linear versus non-linear impression of the EMG–torque relationship of trunk muscles. J Biomech 41:491–497. doi:10.1016/j.jbiomech.2007.10.015

Brown SHM, McGill SM (2009) The intrinsic stiffness of the in vivo lumbar spine in response to quick releases: implications for reflexive requirements. J Electromyogr Kinesiol 19:727–736. doi:10.1016/j.jelekin.2008.04.009

Buchanan JJ, Horak FB (1999) Emergence of postural patterns as a function of vision and translation frequency. J Neurophysiol 81:2325–2339

Cholewicki J, Polzhofer GK, Radebold A (2000) Postural control of trunk during unstable sitting. J Biomech 33:1733–1737

Clauser CE, McConville JT, Young JW (1969) Weight, volume, and center of mass of segments of the human body. Aerospace Medical Research Laboratory. Wright-Patterson Air Force Base, Ohio

Collins JJ, De Luca CJ (1995) The effects of visual input on open-loop and closed-loop postural control mechanisms. Exp Brain Res 103:151–163. doi:10.1007/BF00241972

Day BL, Séverac Cauquil A, Bartolomei L, Pastor MA, Lyon IN (1997) Human body-segment tilts induced by galvanic stimulation: a vestibularly driven balance protection mechanism. J Physiol 500:661–672

Forbes P, Bruijn E, Schouten A, Helm FT, Happee R (2013) Dependency of human neck reflex responses on the bandwidth of pseudorandom anterior-posterior torso perturbations. Exp Brain Res 226:1–14. doi:10.1007/s00221-012-3388-x

Gardner-Morse MG, Stokes IAF (2001) Trunk stiffness increases with steady-state effort. J Biomech 34:457–463. doi:10.1016/s0021-9290(00)00226-8

Goodworth AD, Peterka RJ (2009) Contribution of sensorimotor integration to spinal stabilization in humans. J Neurophysiol 102:496–512. doi:10.1152/jn.00118.2009

Goodworth AD, Peterka RJ (2010) Influence of bilateral vestibular loss on spinal stabilization in humans. J Neurophysiol 103:1978–1987. doi:10.1152/jn.01064.2009

Granata KP, Rogers E (2007) Torso flexion modulates stiffness and reflex response. J Electromyogr Kinesiol 17:384–392

Guitton D, Kearney RE, Wereley N, Peterson BW (1986) Visual, vestibular and voluntary contributions to human head stabilization. Exp Brain Res 64:59–69. doi:10.1007/bf00238201

Halliday DM, Rosenberg JR, Amjad AM, Breeze P, Conway BA, Farmer SF (1995) A framework for the analysis of mixed time series/point process data—Theory and application to the study of physiological tremor, single motor unit discharges and electromyograms. Prog Biophys Mol Biol 64:237–278. doi:10.1016/s0079-6107(96)00009-0

Jenkins GM, Watts DG (1969) Spectral analysis and its applications. Holden-Day, San Francisco

Kiemel T, Elahi AJ, Jeka JJ (2008) Identification of the plant for upright stance in humans: multiple movement patterns from a single neural strategy. J Neurophysiol 100:3394–3406. doi:10.1152/jn.01272.2007

Ljung L (1999) System identification: theory for the user, 2nd edn. PTR Prentice Hall, Upper Saddle River

Loney PL, Stratford PW (1999) The prevalence of low back pain in adults: a methodological review of the literature. Phys Ther 79:384–396

Loram ID, Lakie M (2002) Direct measurement of human ankle stiffness during quiet standing: the intrinsic mechanical stiffness is insufficient for stability. J Physiol 545:1041–1053. doi:10.1113/jphysiol.2002.025049

Moorhouse KM, Granata KP (2007) Role of reflex dynamics in spinal stability: intrinsic muscle stiffness alone is insufficient for stability. J Biomech 40:1058–1065. doi:10.1016/j.jbiomech.2006.04.018

Mugge W, Abbink DA, van der Helm (2007) FCT Reduced power method: How to evoke low-bandwidth behaviour while estimating full-bandwidth dynamics. In: The IEEE 10th international conference on rehabilitation robotics (ICORR), Noordwijk aan Zee (The Netherlands), pp 575–581

Picavet HSJ, Schouten JSAG (2003) Musculoskeletal pain in the Netherlands: prevalences, consequences and risk groups, the DMC3-study. Pain 102:167–178. doi:10.1016/s0304-3959(02)00372-x

Pintelon R, Schoukens J (2001) System identification: a frequency domain approach. Wiley, New York

Radebold A, Cholewicki J, Polzhofer GK, Greene HS (2001) Impaired postural control of the lumbar spine is associated with delayed muscle response times in patients with chronic idiopathic low back pain. Spine 26:724–730

Staudenmann D, Potvin JR, Kingma I, Stegeman DF, van Dieën JH (2007) Effects of EMG processing on biomechanical models of muscle joint systems: sensitivity of trunk muscle moments, spinal forces, and stability. J Biomech 40:900–909. doi:10.1016/j.jbiomech.2006.03.021

Stein RB, Kearney RE (1995) Nonlinear behavior of muscle reflexes at the human ankle joint. J Neurophysiol 73(1):65–72

van der Helm FCT, Schouten AC, de Vlugt E, Brouwn GG (2002) Identification of intrinsic and reflexive components of human arm dynamics during postural control. J Neurosci Methods 119:1–14. doi:10.1016/s0165-0270(02)00147-4

van der Kooij H, Donker S, de Vrijer M, van der Helm F (2004) Identification of human balance control in standing. In: Systems, man and cybernetics, 2004 IEEE international conference on, 10–13 Oct. 2004. vol 2533, pp 2535–2541

van der Kooij H, van Asseldonk E, van der Helm FCT (2005) Comparison of different methods to identify and quantify balance control. J Neurosci Methods 145:175–203. doi:10.1016/j.jneumeth.2005.01.003

van Dieën JH, Selen LPJ, Cholewicki J (2003) Trunk muscle activation in low-back pain patients, an analysis of the literature. J Electromyogr Kinesiol 13:333–351

van Drunen P, Maaswinkel E, van der Helm FCT, van Dieën JH, Happee R (2013) Identifying intrinsic and reflexive contributions to low-back stabilization. J Biomech 46:1440–1446. doi:10.1016/j.jbiomech.2013.03.007

Veldpaus FE, Woltring HJ, Dortmans LJMG (1988) A least-squares algorithm for the equiform transformation from spatial marker co-ordinates. J Biomechan 21:45–54. doi:10.1016/0021-9290(88)90190-X

Willigenburg N, Kingma I, van Dieën J (2010) How is precision regulated in maintaining trunk posture? Exp Brain Res 203:39–49